structure in all those DNA segments. Since the distances between extra-N atoms of adenine and cytosine are long in 5′-TA-3′ and 5′-GA-3′ DNA segments, it is difficult to form DEB(1,3) adducts. DEB(1,4) adducts (see the lower of the cover: The structure of DEB(1,4) cross-linking 5′-GA-3′) of those segments deformed obviously and the complementary base pairs were not yet in the same plane. But the structure of DNA double helix strand still remained to some extent.

DEB easily cross-links with five sequences of DNA in the major groove but only two sequences in the minor groove[8]. Since there were not essential differences in alkylation activity of DEB between two grooves, the selection of sequences increases cross-linking efficiency of DEB in the major groove. The cross-linked DNA is not easily repaired by the mechanism that repairs the single-base alkylating DNA with complementary strand as model. Repaired by the mechanism of deleting the cross-linked DNA double strain at the same time, DNA easily undergoes deletion, frameshift, rearrangement or exchange of sister strain mutation. In the DEB-induced mutation studies[9], there were increased frequencies of mutants by genomic deletion or rearrangement. Also, there were an increased frequency of mutants at A:T pairs compared with the spontaneous mutants. The adduct of DEB alkylating N^4-adenine is in the major groove of DNA. As discussed above, as a bifunctional alkylating agent, DEB can further alkylate the neighbor bases of complementary strand and interstrand cross-link DNA in the major groove. DEB can cross-link with more frequency in major groove than minor groove, which can explain the experimental results[9]. This result is important to "Di-region theory" verification[10].

Meantime, it can be seen that DNA cross-linked with 5′-TA-3′ and 5′-GA-3′ sequences deformed greatly. So these fragments are easily detected and deleted. This might contribute to DEB high mutagenicity also.

Acknowledgements This work was supported by the National Natural Science Foundation of China (Grant No. 29377269).

References

1. Lofroth, G., Burton, M., Forehand, L. et al., Characterization of environmental tobacco smoke, Environ. Sci. Technol., 1989, 23(3): 610.
2. Melnick, R.L., Huff, J., Chou, B.J. et al., Carcinogenicity of 1,3-butadiene in B6C3F1 mice at low exposure concentrations, Cancer Res., 1990, 50(20):6592.
3. International Agency for Research on Cancer (IARC), 1,3-butadiene in occupational exposures to mists and vapors from strong inorganic acids and other industrial chemicals, IARC, 1992, 54(1): 237.
4. Cancer Risk from Outdoor Exposure to Air Toxic, US EPA, Vol. 1 (EPA-450/1-90-004a).
5. Malvoisin, E., Roberfroid, M., Hepatic microsomal metabolism of 1,3-butadiene, Xenobiotica,1982, 12(2): 137.
6. Segal, A., Mate, U., Solomon, J. J., In vitro Dimroth rearrangement of 1-(2-carboxyethyl) adenine to N6-(2-carboxyethyl)adenine in single-stranded calf thymus DNA, Chem. Biol. Interact., 1979, 28(3): 333.
7. Cochrane, J.E., Skopek, T.R., Mutagenicity of butadiene and its epoxide metabolites: Ⅰ. Mutagenic potential of 1,2-epoxybutene, 1,2,3,4-diepoxybutane and 3,4-epoxy-1,2-butanediol in cultured human lymphoblasts, Carcinogenesis, 1994, 15(4): 713.
8. Zhou Zhigang, Dai Qianhuan, Zhong Rugang, Study on metabolites of 1,3-butadiene alkylating and interacting with DNA by AM1, Chemical J. of Chinese University, 1988,19(8) (The Fifth International Symp. For Chin. Org. Chem.): 397.
9. Ann-Marie, Steen., Kathy, G. M., Leslie, R., Analysis of hprt mutations occurring in human TK6 lymphoblastoid cells following exposure to 1,2,3,4-diepoxybutane, Mutagenesis, 1997, 12(2): 61.
10. Dai Qianhuan., Di-region theory, new discovery on mechanism of carcinogenesis, Mol. Eng., 1998, 8(1): 1.

(Received February 12, 1999)

Surface interactions of MoO_3/α-Fe_2O_3 system

XU Fei, HU Yuhai, DONG Lin & CHEN Yi

Department of Chemistry, Institute of Mesoscopic Solid State Chemistry, Nanjing University, Nanjing 210093, China

Abstract α-Fe_2O_3-supported molybdena catalysts have been prepared by heating a mixture of MoO_3 and α-Fe_2O_3. XRD, XPS, LRS, TG-DTA and Mössbauer spectroscopy were used to characterize the interactions between MoO_3 and α-Fe_2O_3. The dispersion capacity of MoO_3 on the surface of α-Fe_2O_3 determined by XRD and XPS was 0.8 mmol/100m^2 α-Fe_2O_3 in the samples calcined at 420℃. For the sample with low MoO_3 loading, LRS and FT-IR results showed that Mo^{6+} ions were located in the tetrahedral vacant sites on the surface of α-Fe_2O_3, signed as Mo-Ⅰ.

The amount of Mo-II species, formed by Mo^{6+} ions incorporated into the octahedral vacant sites, increased with the MoO_3 loading. Based on the assumption that the (001) plane of α-Fe_2O_3 is preferentially exposed, almost all the Mo_{6+} ions of the dispersed molybdena species existed at the surface octahedral sites for the sample with MoO_3 loading close or beyond the dispersion capacity, and formed the Mo-II species. In this case, the capping O^{2-} ions linking with the incorporated Mo^{6+} ions formed a surface epitaxial structure, which was in good agreement with the results predicted by the incorporation model proposed previously. XRD and Mössbauer spectroscopy of the MoO_3 / α-Fe_2O_3 samples calcined at different temperatures showed that the calcination temperature could strongly influence the interaction extent: (i) at 420℃, MoO_3 dispersed on the surface of α-Fe_2O_3 and formed surface Mo species; (ii) at 500℃, MoO_3 reacted with the bulk of α-Fe_2O_3 and formed $Fe_2(MoO_4)_3$ compound.

Keywords: MoO_3, α-Fe_2O_3, surface interaction , dispersion capacity.

The surface interaction between the active components and their supports is a key subject in catalysis. Many investigations of the system with metal oxides supported on γ-Al_2O_3, SiO_2, TiO_2, ZrO_2, CeO_2, etc., have been carried out[1−4], which supplied useful information for understanding of the interaction mechanism of such catalysts.

Ferric oxides and ferric compounds are widely used in the preparation of magnetic materials, active components of catalysts, absorbents and pigments[5]. α-Fe_2O_3, as the high temperature stable crystalline in the ferric oxide compounds, has a hexagonal structure of densely averaged oxygen atoms, which is suitable for studying the physicochemical properties of α-Fe_2O_3-supported catalysts. However, few reports about systems with α-Fe_2O_3 as a supporter have been found[6].

In this note, α-Fe_2O_3 with a Brunauer-Emett-Teller (BET) surface area of 55 m^2/g after calcination at 550℃ for 5 h was used as a supporter to prepare MoO_3 / α-Fe_2O_3 samples. XRD, XPS, LRS, Mössbauer spectroscopy and TG-DTA were applied to investigating the dispersion of MoO_3 on α-Fe_2O_3 as well as the effects of temperature change on the interaction extent of MoO_3 and α-Fe_2O_3. The results showed that MoO_3 only dispersed on the surface of α-Fe_2O_3 and formed surface "Mo-O" species when the calcination temperature was at 420℃, and the compound, $Fe_2(MoO_4)_3$, had been formed as the temperature rose to 500℃. All the results were discussed by using the incorporation model.

1 Experimental

(i) Instruments. The BET surface area of α-Fe_2O_3 was measured on a Micromeritics ASAP-2000 instrument. XRD results were recorded using a Shimadzu XD-3A X-ray diffractometer with FeK_α radiation and an Mn filter. α-alumina powder was used as a reference for quantitative analysis. XPS results were obtained on a V. G. Escalab MK II spectrometer equipped with a hemispherical electron analyzer, MgK_α radiation (1 253.6 eV) was operated at 15 kV and 20 mA, samples were analyzed in the constant pass energy mode at 20 eV, C_{1s} (285 eV) was taken as a reference to calculate the binding energies (BE). LRS were obtained with a Spex Ramalog 1403 spectrometer. The 488 nm line and laser source power of 200 mW and the laser power of 15−20 mW at the sample were used, and the scanning velocity was 2 $cm^{-1} \cdot s^{-1}$. Mössbauer spectroscopy was performed with a constant acceleration spectrometer using a 10 mCi $^{57}Co/Pd$ source, α-Fe was used to demarcate the velocity. TG-DTA experiments were carried out on a Rigaku thermoanalyzer (Japan), with α-Al_2O_3 as a refer- ence. The temperature was increased linearly at a rate of 20℃ • min^{-1}.

(ii) Samples. α-Fe_2O_3 supplied by Shanxi Coal and Chemistry Institute was calicined at 550℃ for 5 h, the BET surface area was 58 $m^2 \cdot g^{-1}$. XRD results indicated that iron oxide is pure hexagonal crystalline. MoO_3(AR) produced by Shanghai Coll- oid Chemistry Factory was also calcined at 400℃ for 5 h and sieved to 200 meshes before used for sample preparation. A series of samples with different MoO_3 loading labeled "X mmol/100 m^2 α-Fe_2O_3" were prepared by calcining the mixtures of MoO_3

and α-Fe_2O_3 in air stream at 420 or 500℃ for 24 h.

2 Results and discussions

(i) Dispersion of MoO_3 on the surface of α-Fe_2O_3 at 420℃. Fig. 1 shows the XRD patterns of a series of MoO_3 / α-Fe_2O_3 samples with different MoO_3 loading before and after calcination for 24 h. Peaks corresponding to crystalline MoO_3 were observed (2θ=29.46°, 34.58°) in all the mixtures before calcination in patterns 1, 2 and 3, while these peaks disappeared in the samples with MoO_3 loading of 0.3 and 0.6 mmol/100 m^2 α-Fe_2O_3 after calcination in patterns 1′, 2′. It is likely that MoO_3 had dispersed on the surface of α-Fe_2O_3. For the sample of 1.0 mmol/100 m^2 α-Fe_2O_3 as shown in pattern 3′, peaks of crystalline MoO_3 still remained despite of calcination, but the peak intensity decreased as seen by comparing patterns 3′ and 3. The result illustrated that some residual crystalline MoO_3 still existed besides the partially dispersed MoO_3 on α-Fe_2O_3 in this sample. Furthermore, XRD quantitative analysis[7] of the system indicated that the dispersion capacity of MoO_3 on α-Fe_2O_3 is 0.8 mmol/100 m^2 α-Fe_2O_3.

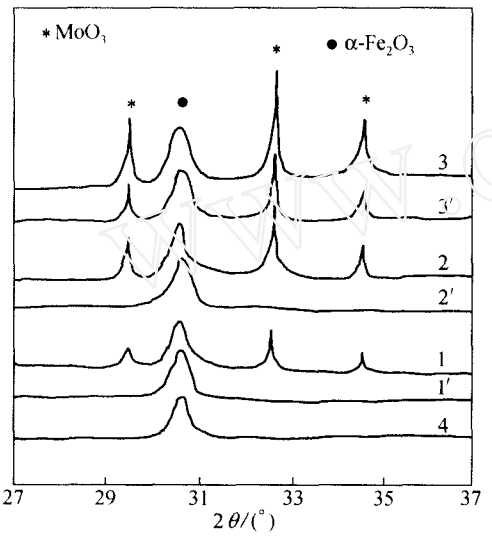

Fig. 1. XRD patterns of MoO_3/α-Fe_2O_3 samples.

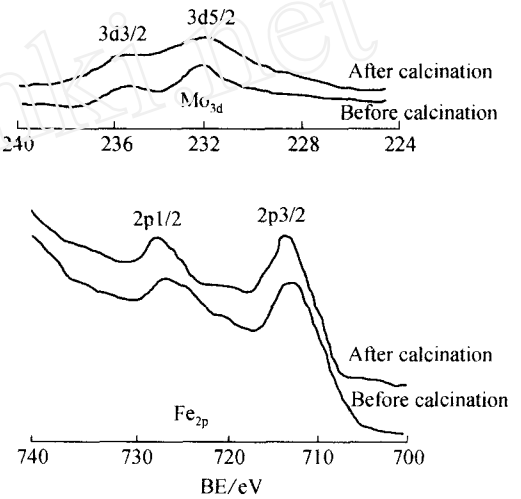

Fig. 2. XPS results of Fe_{2p} and Mo_{3d} in MoO_3/α-Fe_2O_3 samples.

XPS results of Fe_{2p} and Mo_{3d} in the sample with MoO_3 loading of 0.6 mmol/100 m^2 α-Fe_2O_3 are shown in fig. 2. The XPS intensity ratio of Mo to Fe, I_{Mo} / I_{Fe}, changed more quickly for the sample after calcination, which increased from 0.08 to 0.22, indicating that heat treatment made MoO_3 better dispersed on the surface of α-Fe_2O_3 to form the surface Mo species[8]. However, the BE of $Fe_{2p3/2}$ and $Mo_{3d5/2}$ did not change by calcination, which meant that the valances of Fe and Mo still kept +3 and +6 respectively.

Fig. 3 shows the LRS results that MoO_3 mainly dispersed on the surface of α-Fe_2O_3 in the samples with MoO_3 loading lower than its dispersion capacity. For the sample of 0.3 mmol/100 m^2 α-Fe_2O_3, two peaks at 815 and 880 cm^{-1} were observed (fig. 3-2). And another peak at 939 cm^{-1}appeared (fig. 3-3) besides the two peaks at 813 and 878 cm^{-1}, which illustrated that there might be more than one type of surface Mo-O species existing[9]. However, for the sample with MoO_3 loading of 1.0 mmol/100 m^2 α-Fe_2O_3 (fig. 3-4), the peak at 880 cm^{-1} could not be observed and the peak intensity of 939 cm^{-1} increased as compared with fig. 3-3. Considering that the (001) plane of α-Fe_2O_3 is preferentially exposed[10], in each unit mesh of α-Fe_2O_3, besides two of the octahedral vacancies that have been occupied by Fe^{3+} ions, as shown in fig. 4(a), there are three tetrahedral and one octahedral vacant sites left for the Mo^{6+} ions to incorporate in and the surface Mo species can be formed. In this

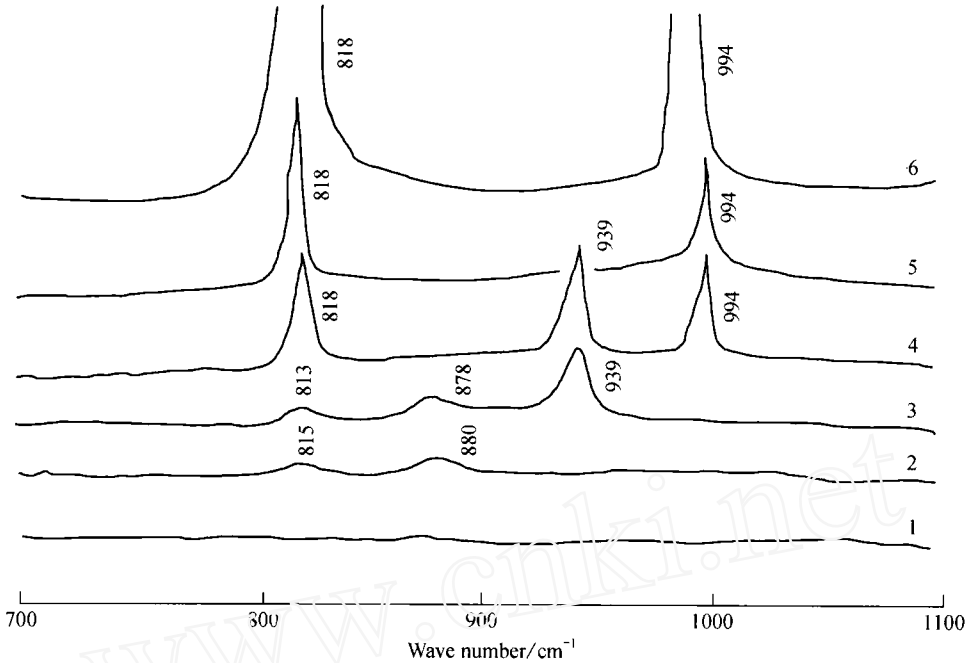

Fig. 3. LRS result of MoO_3/α-Fe_2O_3 samples.

model, two kinds of Mo species with different coordination environments could be formed: Mo^{6+} ions in the tetrahedral vacant sites (Mo-Ⅰ), and Mo^{6+} ions in the octahedral vacant sites (Mo-Ⅱ). Though they were both six-coordinated O^{2-} ions, the interaction between the incorporated Mo^{6+} ions and the surrounding Fe^{3+} ions was different. Furthermore, considering the ratio between the surface vacancies (tetrahedral vacancies/octahedral vacancies) being 3∶1, there is a higher possibility of Mo^{6+} ions entering the tetrahedral vacancies with low MoO_3 loading, which could be supported by the LRS results. Note that the peaks at 815 and 880 cm^{-1}, representing Mo-Ⅰ species, appeared (fig. 3-2) for the sample with low MoO_3 loading, and for the sample with MoO_3 loading of 1.0 mmol/100 m^2 α-Fe_2O_3 (fig. 3-4), the peak at 880 cm^{-1} disappeared, replaced by the peak of 939 cm^{-1}, which should be corresponding to the formation of Mo-Ⅱ species. In this case, an epitaxial capping O^{2-} structure was formed on the (001) plane of α-Fe_2O_3, as shown in fig. 4 (b).

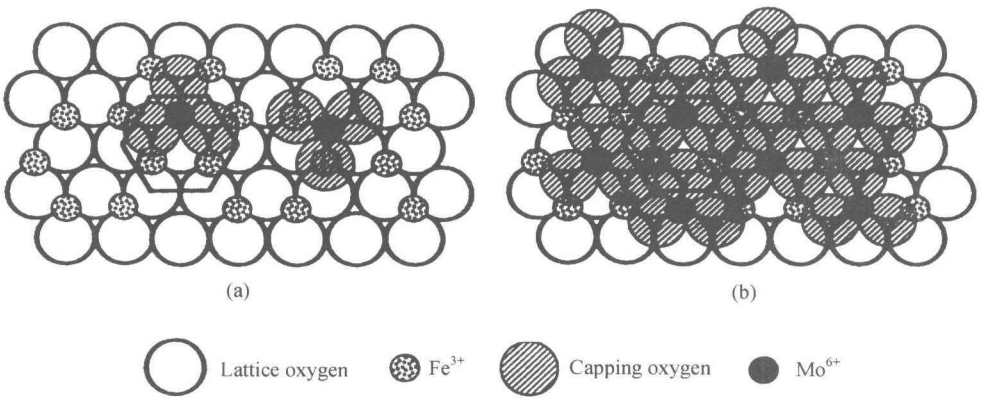

Fig. 4. Configuration of surface Mo-O species on MoO_3/α-Fe_2O_3 samples.

(ii) Temperature influence on the interaction between MoO_3 and α-Fe_2O_3. XRD patterns of the sample with MoO_3 loading of 2.0 mmol/100 m^2 α-Fe_2O_3 after calcination at 420 and 500℃ are shown in fig. 5. At 500℃, peaks corresponding to crystalline MoO_3 disappeared and the intensity of the peaks representing α-Fe_2O_3 decreased as seen by comparing patterns 2 and 2′(fig. 5); meanwhile, a new peak (2θ=28.9°) corresponding to $Fe_2(MoO_4)_3$ appeared. It is thus deduced that a strong interaction between MoO_3 and α-Fe_2O_3 occurred at this temperature, so that a new compound $Fe_2(MoO_4)_3$ was formed. Mössbauer results of the sample with MoO_3 loading of 2.0 mmol/100m^2 α-Fe_2O_3 calcined at different temperatures are shown in fig. 6, and Mössbauer parameters listed in table 1.

For the sample treated at 420℃, the parameters were similar to those of pure α-Fe_2O_3. The hyperfine field decreased and a new single peak corresponding to $Fe_2(MoO_4)_3$ species appeared as the temperature rose to 500℃. This result was in agreement with that by XRD. It was suggested that the decrease of the hyperfine field was attributed to the formation of $Fe_2(MoO_4)_3$ phase which covered the α-Fe_2O_3 particles to form a so-called "heart-wrapping spe- cies", as shown in fig. 7. The decreased hyperfine field of α-Fe_2O_3 resulted from the decrease of the size of α-Fe_2O_3 particles, which was in good agreement with the results reported elsewhere[11]. TG-DTA experiments were carried out to monitor the process of MoO_3 dispersing on α-Fe_2O_3 by heat treatment. Four endothermic peaks at 400, 457, 634 and 700℃ appeared in the DTA curve as shown in fig. 8. Studying the combined XRD and Mssbauer results attributed the above peaks: that at 400℃ to the diffusion of MoO_3 on the α-Fe_2O_3 surface, at 457℃ to the reaction of MoO_3 and the bulk of α-Fe_2O_3, at 700℃ to the sublimation of molybdenum oxides, that at 634℃ was yet to be determined. The TG curve was flat from 300℃ to 700℃, which meant that no mass change happened during the process. An evident weight loss was observed when the temperature rose to 700℃, which was due to the sublimation of Mo-O oxides. This suggestion was supported by the blue molybdenum oxides appearing on the wall of the sample cell after the experiments.

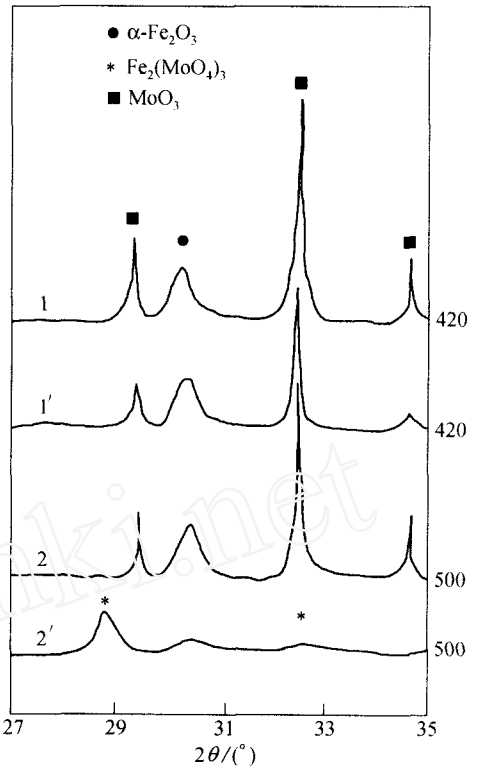

Fig. 5. XRD patterns of MoO_3/α-Fe_2O_3 samples before and after calcination at 420 and 500℃.

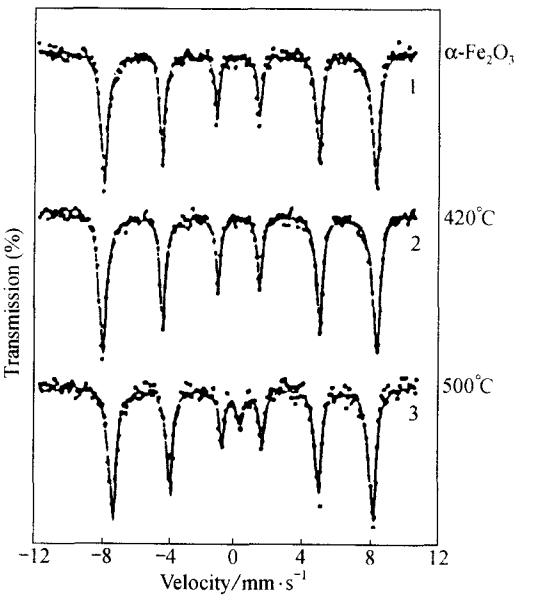

Fig. 6. Mössbauer spectroscopy of MoO_3/α-Fe_2O_3 sample.

Table 1 Mössbauer parameters of MoO_3/α-Fe_2O_3 sample

Sample	Treatment	IS/mm • s^{-1}	QS/mm • s^{-1}	H/A • m^{-1}	Iron species
α-Fe_2O_3	500℃	0.39	0.17	4.05×10^7	α-Fe_2O_3
MoO_3/α-Fe_2O_3	420℃	0.42	0.12	4.02×10^7	α-Fe_2O_3
MoO_3/α-Fe_2O_3	500℃	0.47	0.18	3.84×10^7	α-Fe_2O_3
		0.51	0	0	$Fe_2(MoO_4)_3$

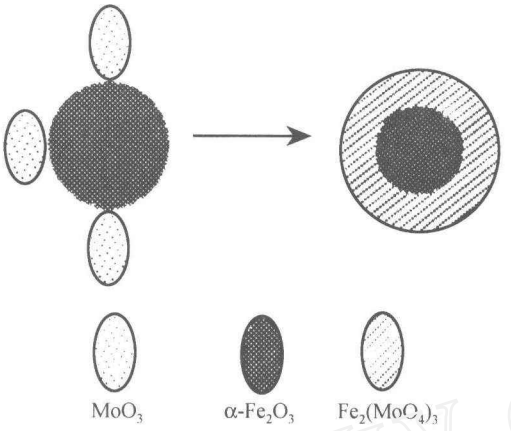

Fig. 7. $Fe_2(MoO_4)_3$ formed in MoO_3/α-Fe_2O_3 sample.

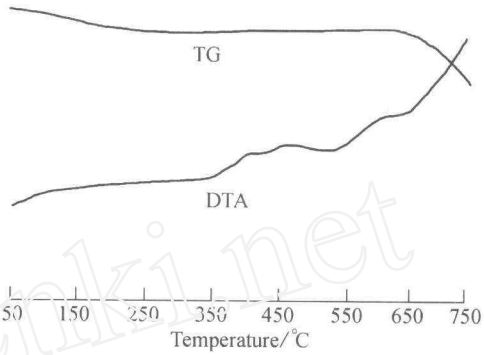

Fig. 8. TG-DTA results of MoO_3/α-Fe_2O_3 sample.

3 Conclusion

The dispersion capacity of MoO_3 on the α-Fe_2O_3 surface was 0.8 mmol/100 m^2 α-Fe_2O_3 after suitable heat treatment. For the samples with MoO_3 loading lower than its dispersion capacity, MoO_3 well dispersed on the surface of α-Fe_2O_3 to form surface Mo species, Mo-Ⅰ or/and Mo-Ⅱ, and the environments of incorporated Mo^{6+} ions were different though they were all six-coordinated with O^{2-} ions. However, some residual crystalline MoO_3 existed in the samples as the MoO_3 loading was beyond its dispersion capacity.

XRD, Mössbauer and TG-DTA results showed that MoO_3 in reaction with α-Fe_2O_3 produced a new compound $Fe_2(MoO_4)_3$ when MoO_3/α-Fe_2O_3 samples had been treated at 500℃, which suggested that the calcination temperature could strongly influence the interaction extent between MoO_3 and α-Fe_2O_3.

Acknowledgements The authors thank Prof. Zhong Bing for kindly supplying the high surface α-Fe_2O_3. This work was supported by Chinese Special Doctoral Foundation (Grant No. 98028434) and the Modern Analysis Central Foundation of Nanjing University.

References

1. Knozinger, H., Taglauer, E., Toward supported oxide catalysts via solid-solid wetting, in Catalysis (eds. Spivey, J. J., Agarwal, S. K.), London: The Royal Society of Chemistry, 1993, 10: 1.
2. Xie, Y. C., Tang, Y. Q., Spontaneous monolayer dispersion of oxides and salts onto surfaces of supports: applications to heterogeneous catalysis, Adv. Catal., 1990, 37: 1.
3. Dong, L., Jin, Y. S., Chen, Y., Dispersion state of CuO on CeO_2, Science in China, Ser. B, 1997, 40(1): 24.
4. Dong, L., Hu, J. Q., Xu, B. et al., Surface state of molybdenum cations in MoO_3/CeO_2, Chinese Science Bulletin, 1997, 42(13): 1406.
5. Rao, C. N. R., Transition Metad Oxides in Solid State Chemistry, New York: Marcel Dekker, 1974, 455.
6. Yamada, H., Niwa, M., Murakami, Y., Methanol oxidation on a molybdena monolayer supported on iron oxide, Appl. Catal. A. General, 1993, 96: 113.
7. Xie, Y. C., Tang, Y. Q., Adv. Catal. (in Chinese), Xiamen: Xiamen University Press, 1996, 142.
8. Gui, L. L., Liu, Y. J., Application of XPS to study the dispersion and surface state for MoO_3 supported on the surface of TiO_2, ν-Al_2O_3 and SiO_2, Science in China, Ser. B, 1985, 28(12): 1233.
9. Ng, K. Y. S., Gulari, E., Molybdena on titania, Part. I. J. Catal., 1985, 92: 340.
10. Knozinger, H., Specific poisoning and characterization of catalytically active surface, Adv. Catal., 1976, 25: 185
11. Kunding, W., Bommel, H., Constabaris, G. et al., Some properties of supported particles determined with Mössbauer effec, Phys. Rev.,1966, 142: 327.

(Received April 19, 1999)